Proceedings of IMECE'03
2003 ASME International Mechanical Engineering Congress
Washington, D.C., November 15–21, 2003

IMECE2003-43837

FORMATION OF MICROSCOPIC VOIDS IN RESIN TRANSFER MOLDED COMPOSITES

Youssef K. Hamidi Levent Aktas M. Cengiz Altan*
School of Aerospace and Mechanical Engineering
University of Oklahoma
Norman, OK 73019
*e-mail: altan@ou.edu

ABSTRACT

Performance of composite materials usually suffers from process-induced defects such as dry spots or microscopic voids. While effects of void content in molded composites have been studied extensively, knowledge of void morphology and spatial distribution of voids in composites manufactured by resin transfer molding (RTM) remains limited. In this study, through-the-thickness void distribution for a disk-shaped, E-glass/epoxy composite part manufactured by resin transfer molding is investigated. Microscopic image analysis is conducted through-the-thickness of a radial sample obtained from the molded composite disk. Voids are primarily found to concentrate within or adjacent to the fiber preforms. More than 93% of the voids are observed within the preform or in a so-called transition zone, next to a fibrous region. In addition, void content was found to fluctuate through-the-thickness of the composite. Variation up to 17% of the average void content of 2.15% is observed through-the-thicknesses of the eight layers studied. Microscopic analysis revealed that average size of voids near the mold surfaces is slightly larger than those located at the interior of the composite. In addition, average size of voids that are located within the fiber preform is observed to be smaller than those located in other regions of the composite. Finally, proximity to the surface is found to have no apparent effect on shape of voids within the composite.

INTRODUCTION

Due to its versatility and low cost, resin transfer molding has been a popular method for manufacturing near-net-shape, geometrically complex, composite parts. Although the majority of load-bearing structural composite components in aerospace industry are fabricated by traditional autoclave process, automotive industry utilizes RTM for structural or semi-structural parts due to lower operational cost and higher production rates [1]. Resin transfer molding and its variants consist of injecting a thermosetting polymeric resin into a mold cavity preloaded with a multi-layer, fibrous reinforcing preform. During mold filling, the resin wets individual fibers and pushes air out of the mold cavity through the exit gates. As the fluid front impregnates the fibrous preform, dry spots and microscopic voids may be formed in or near the fiber tows due to incomplete wetting of the preform. The formation of such microscopic voids during resin injection is one of the major barriers to larger scale usage of these molding processes.

Detrimental effect of voids on mechanical performance of composites is well established. Judd and Wright [2], for example, reported that a void content as low as 1% results in a decrease in strength up to 30% in bending, 3% in tension, 9% in torsional shear, and 8% in impact. In a more recent study of voidage effects on mechanical properties, Goodwin et al. [3] reported a 7% reduction in interlaminar shear strength per 1% increase in voidage up to 10% for a resin transfer molded composites containing 5-harness satin preform. In addition, the authors observed that failure cracks initiate from medium to large sized voids with sharp corners, but not from small spherical voids. Voidage is also known to affect both the rate and equilibrium level of moisture absorption in composite parts [4].

Lowering or totally eliminating voids in RTM parts involves understanding mechanics of void formation during filling of the mold cavity. In resin transfer molded composites, voids are reported to originate primarily from mechanical entrapment during mold filling [5-8]. In some cases, voids can also emerge from volatilization of dissolved gases in the resin, partial evaporation of mold releasing agent into the preform, and initial air bubble content in the resin [9].

The mechanical entrapment is believed to arise from the presence of alternative paths for resin flow as a result of non-homogeneous preform permeabilities. The non-homogeneity in preform permeability leads to the following two different flow fields: (a) viscous flow through the opening between fiber bundles, and (b) capillary flow where resin penetrates into fiber bundles. At slower injection flow rates, the capillary flow within the fiber tows leads the viscous flow and promotes intra-tow void entrapment at the interstices of the tow structure. In contrast, high injection flow rates promote inter-tow void entrapment within fiber bundles as viscous flow leads capillary flow during preform impregnation. A comprehensive analysis of this phenomenon has often been performed [5-9] using the capillary number, *Ca*, defined as the non-dimensional ratio of the viscous forces to the capillary forces:

$$Ca = \frac{\mu V}{\gamma}, \tag{1}$$

where μ, V, and γ are the impregnating resin viscosity, the macroscopic fluid front velocity, and the resin surface tension, respectively.

A correlation between overall void content and capillary number is well-established in the literature [5-9]. Mahale et al. [6] reported that below a certain capillary number critical value (i.e. $Ca < 2.5 \times 10^{-3}$), void content augments exponentially with decreasing capillary number during planar radial flow into non-woven multifilament glass networks. Moreover, if capillary number is above this critical value, negligible void entrapment was reported. Incorporating the liquid-fiber-air contact angle into the non-dimensional capillary number was found to help generalize the analysis by preventing discrepancies caused by material variation. The resulting modified capillary number, Ca^*, has been defined by Patel et al. [7] and Rohatgi et al. [8] as:

$$Ca^* = \frac{\mu V}{\gamma \cos\theta}, \tag{2}$$

where θ is the advancing contact angle. Both references reported the existence of a single master curve of void content plotted as a function of the modified capillary number. Experimentally measured data followed this master curve for various model fluids injected at different fluid velocities. They also reported the existence of a preferential range of modified capillary number between 10^{-3} and 10^{-2}, within which intra-tow macro-voids and inter-tow micro-voids coexist. Below this preferential range ($Ca^* < 10^{-3}$), voids are primarily intra-tow macro-voids, and above the second critical value of 10^{-2}, voids are mainly micro-voids trapped inside fiber bundles.

In order to predict void formation during mold filling, a number of authors developed theoretical and numerical models [10-15]. Most of the proposed models introduced numerous assumptions, and often considered simplified preform architectures. For instance, Chan and Morgan [10] developed a model that predicts localized void formation at the resin front region, but only for unidirectional preforms with parallel flow. Chui et al. [11], on the other hand, proposed a theoretical model predicting a voidage-pressure dependence in RTM processes. Although the model was based on a simple unsaturated flow in porous media, the voidage-pressure dependence was confirmed experimentally by Lundström [12]. Patel and Lee [13,14] also developed a model for void formation in liquid composite molding (LCM) processes based on the multi-phase Darcy's law. Furthermore, a simple analytical model for tow impregnation when the macroscopic flow is parallel to the fiber axis was developed by Binetruy et al. [15]. Additionally, several researchers [16,17] investigated bubble motion through constricted micro-channels to characterize void transport through fiber reinforcement. Lundström [16] reported that voids are more prone to mechanical entrapment within fiber bundles than between bundles. Shih and Lee [17] found that bubble mobility depends on both bubble size and the resin-fiber contact angle.

Proposed void reduction methods for RTM composites in the literature include vacuum assistance [18], continuing the resin flow after complete wet out [5], compressing mold walls during injection [19], and applying a permanent post fill pressure after injection [20,21]. Nevertheless, the most effective technique for void reduction cannot be established without thorough understanding of the spatial void distribution throughout the composite part. To the best of the authors' knowledge, such detailed spatial void characterization has not yet been available for resin transfer molded composites. In the current work, we study the spatial void distribution and void morphology in a disk-shaped, E-glass/epoxy composite fabricated by resin transfer molding. A radial sample from this disk is analyzed through-the-thickness by an optical microscope. In addition, since void size and shape are critical both in failure mechanisms [3] and in void mobility during injection [17], their variations in the thickness direction are investigated.

EXPERIMENTAL STUDIES

Procedure for composite manufacturing

An epoxy resin, EPON 815C (Shell Chemicals) is chosen as the molding material. Attractive characteristics of this resin include low toxicity and low viscosity, suitable for effective preform impregnation and lower injection pressures. The gel time of about 20 minutes is obtained by choosing the curing agent EPICURE 3282 (Shell Chemicals). As depicted in figure 1, the apparatus used to fabricate resin transfer molded disks comprises a molding press and a disk-shaped mold cavity. The molding press contains a 40-ton hydraulic press (ARCAN, Model CP402), and two hollow cylinders, designed

for resin and curing agent, respectively. The internal diameters of the two stainless steel cylinders are machined to 55.47 and 25.53 mm in order to realize the exact mix ratio of 4.7 to 1 by volume of resin to curing agent. When the hydraulic press is activated, the attached plungers progress at a constant linear velocity of 2 x 10^{-3} m/s. The flows from the two cylinders coalesce through a T-connector. Subsequently, the resin and curing agent mixture pass through a Statomix® static inline mixer (ConProTec, Inc., 32 segments. L=155 mm, ID= 5 mm, OD= 8mm). The mixture is afterwards injected through the center of the disk-shaped cavity at a constant injection rate of 5.32 cm^3/s. The mold cavity, as shown in figure 1, is built by placing a 3.18 mm-thick aluminum spacer plate between two 12.6 mm-thick aluminum mold walls. A 152.4 mm diameter circle is cut from the center of the spacer plate to form the disk-shaped cavity. A centered inlet gate and four symmetrically positioned vents are placed on the top mold wall. Leakage is prevented by placing 4-mm O-rings into machined grooves in each mold wall. The filling pressure steadily increases as the flow front advances radially outward towards the exit vents by impregnating random-fiber preform. The exit vents are intentionally placed at a diameter of 177.8 mm to force the resin into the narrow opening between mold walls and spacer plate. Hence, after the mold cavity is full, the pressure increases at a very steep rate as the resin creeps inside this tight space. The pressure reaches a maximum inside the mold, as higher pressure is expected to ensure the full impregnation of the dry preform, help reduce voidage [11-12], and facilitate void mobility [17]. Once the pressure reaches a high-enough value, resin starts to come out of the exit vents. Resin injection is then immediately stopped, and exit vents are left unclamped to allow continued discharge of the resin until the driving pressure gradient becomes zero. The reinforcement used in this study is a chopped-strand, randomly-oriented E-glass fiber mat, having a planar density of 0.459 kg/m^2 (Fiberglast, part #250). Four layers of preform are cut into 152.4 mm diameter circles and placed into the mold cavity preceding filling. After resin comes out of all four exit vents, the part is left to cure in the mold for 48 hours before demolding. The part is then post cured at room temperature for two extra weeks to achieve total cross-linking. The resulting product is a 3.88 mm-thick resin transfer molded composite disk having 152.4 mm diameter, with an 18.1% fiber volume fraction. Because of the planar randomness of the preform and the disk axisymmetry, the void morphology within the sample is expected to be independent of the angular position. Therefore, spatial void distribution is investigated only through-the-thickness of a radial specimen from the molded disk.

Capillary number determination

As discussed in the introduction, void content is known to correlate well with the capillary number [5-8]. In addition, the modified capillary number is helpful in understanding the effect of micro-scale flow during fluid front progression. Determining the modified capillary numbers involved in mold filling is needed to identify void formation mechanisms, and consequently spatial void distribution within the molded disk.

Determining the modified capillary number requires, as described in equation 2, quantifying the resin viscosity, μ, the macroscopic fluid front velocity, V_{ave} , the resin surface tension, γ, and the advancing contact angle, θ. Both the surface tension and the advancing contact angle are measured in an earlier study for the same system of resin, curing agent, and E-glass-fibers [21]. The respective measured values of the surface tension and advancing contact angle are 36.3 x 10^{-3} N/m, and 34°. The viscosity of the resin-curing agent mixture is measured using a Brookfield viscometer (Model DV-II +). Even though the mixture's viscosity changes a great deal towards the end of the 20 minute gel time, its value remains reasonably stable around 0.96 $N{\cdot}s/m^2$ during the first few minutes of mixing. The macroscopic fluid front velocity can be determined from the injection flow rate and the mold geometry as:

$$V_{ave} = \frac{Q}{A} = \frac{Q}{2\pi H r(1 - V_f)}, \tag{3}$$

where Q is the resin flow rate, H is the thickness of the mold, r is the radius at which the capillary number is calculated, A is the cross-sectional area of the resin flow at r, and V_f is the fiber volume fraction. Substituting equation 3 in equation 2, the modified capillary number becomes a function of the radial distance from the injection gate:

$$Ca^* = \frac{\mu Q}{2\gamma\pi H(1 - V_f)\cos\theta} \cdot \frac{1}{r}. \tag{4}$$

Void characterization

Microscopic image analysis is utilized to investigate average void content and spatial void distribution through-the-thickness of the composite disk. Microscopic image analysis is chosen since it is believed to be among the most accurate methods for measuring the true void content [22]. Moreover, image analysis offers the advantage of providing detailed information of other important parameters such as void location and void shape and size distribution that cannot be assessed by any other method. However, voidage measurement by optical imaging is generally performed on limited sample surface area. Statistical averaging is also commonly used from random acquisition of pictures over the larger area of interest. Image analysis in the current work, on the other hand, is performed over the entire cross-sections studied, and hence all identifiable voids at the working magnification are included in the void analysis.

In order to investigate the void distribution through-the-thickness, a radial specimen is cut from the cured composite

disk. The length and thickness of the specimen are 75 and 3.88 mm, respectively. Once embedded into a quick cure acrylic resin (Allied High Tech. Products, part # 170-10000), the sample is polished in six successive steps with a series of polishing pastes (Clover Compound) with grits sizes ranging from 180 (e.g. 80 μm average particle diameter) to 1200 (15 μm). After each step, the sample is sonicated for 40 minutes in an ultrasonic cleaner (50 kHz) to remove all residues of the polishing compound.

The optical image analysis starts by dividing the 3.88 mm-thick specimen into eight layers through-the-thickness (seven 0.5 mm-thick layers and one 0.38 mm-thick bottom layer). Frames captured from different 0.5 mm-layers are used to assess the voidage distribution through the specimen thickness. Each layer is then entirely scanned at 200x magnification using a MEIJI optical microscope. At this particular magnification, every frame displayed about 0.71 x 0.53 mm^2 area. Hence, scanning across the sample thickness at a particular radial location needs the capture of eight frames. Images of each layer containing an identified void are captured using a PC-based CCD camera. A total of approximately 460 frames containing voids are captured during this analysis. Each picture is processed using the image analysis software UTHSCSA Image Tool®, which allows the measurement, for each void, of the area, A, and the maximum length, L_{max}. Void contents of different layers are then calculated.

RESULTS AND DISCUSSION

Location of voids and average void content

The voids observed in the molded part are located in three different void zones. First zone is defined as those areas that are rich in matrix and not comprising any fiber preform. Voids located in this zone are completely surrounded by the epoxy matrix and referred to as matrix voids. Second zone is defined as fiber rich-region where the area is dominantly composed of reinforcing preform. Voids in this region are situated within fiber bundles and are referred to as preform voids. Finally, transition zone is defined as the zone between the two other zones herein defined. Voids located in this zone are referred to as transition voids and are always positioned adjacent to fiber bundles but not inside the preform. Figure 2 depicts sample images containing voids obtained from the three defined zones at 200x magnification. In figure 2(a), the continuous polymeric matrix appears as a gray background, the white circular and elliptical objects correspond to glass fibers oriented perpendicularly and in an angle, respectively, to the cross-section. The white parallel stripes represent glass fibers parallel to the studied cross-section. Based on the void locations defined earlier, the two voids present in figure 2(b) are matrix voids. The five voids appearing in figure 2(c), on the other hand, fall into the category of preform voids. Finally, the adjacent void to fibers seen in figure 2(d) is considered a transition void. Voids from these three different zones are identified and their respective contributions to the overall void content determined in order to investigate likelihood for void mobility. In addition, classifying voids based on their proximity to fibers can help estimate their primary effect on mechanical properties. It is known that matrix voids only reduce the load-bearing composite cross-section, while preform and transition voids also weaken local fiber-matrix adhesion.

Combining all through-the-thickness layers, an average void content of 2.15% is calculated. As depicted in figure 3, matrix voids make up only 0.15%, thus form only 6.98% of the total voidage of 2.15%. On the other hand, transition and preform voids make up most of the void content with 1.31 and 0.72%, respectively. The modified capillary number, as discussed in the introduction, can be used to help understand the void formation mechanisms involved in the micro-scale flow during fluid front progression leading to this specific zone distribution. Substituting the previously measured values of 36.3 x 10^{-3} N/m for surface tension, and 34° for advancing contact angle in equation 4, the modified capillary number is found to vary between 0.13 and 1.15 along the radial distance from the injection gate. Those values suggest that the formed voids should be mostly inter-tow micro-voids [7], which is consistent with the results seen on figure 3. As figure 3 illustrates, preform and transition voids combined represent 93.02% of the total voidage formed within the composite part.

Variation of void content through-the-thickness

Non-uniformity in voidage through-the-thickness of the composite disk can arise from uneven spaces between the preform layers, or between the preform and the mold walls. It can also originate from the possible change in the velocity of fluid front between mid-plane and other planes. Another plausible cause can be the poor wettability of the aluminum mold walls pretreated with Teflon mold releasing agent. To quantify the void content change through the specimen's thickness, eight layers are defined as described earlier, with the first layer defined as the very top 0.5 mm-thick layer. Note that the eighth layer is only 0.38 mm-thick. Void contents obtained for these eight different layers are shown in figure 4. Void contents are found to vary significantly from one layer to another, between a maximum of 2.62% in layer 4 and a minimum of 1.25% in the eighth layer. A standard deviation of 0.53% was calculated yielding a 95% confidence interval of 0.37%, which represents 17.21% of the average void content. Consequently, the commonly used statistical averaging of void contents calculated from randomly acquired pictures may introduce 17% error in the overall void content. Thus, scanning the whole cross-section may be needed in order to obtain an accurate overall void content. For the remaining part of the study, the eight layers are combined into two major layers to summarize the results as we focus on other voidage aspects. The first layer is combined with the

seventh and eighth layers to define a surface layer, which represents the composite regions right next to the mold walls surface. Voids found within these layers are referred to as surface voids. The second, third, fourth, fifth, and sixth layers are combined into an inner layer representing the layers within the composite's core, away from mold walls effects. Voids encountered within these layers are called inner voids.

Variation of void size

Classifying void sizes is essential in the choice of void removal method as size is reported to affect void mobility [17]. Larger voids have longer perimeters and thus have larger adhesion force; small voids, on the other hand, have lower adhesion force and therefore become more mobile. Captured void surface area data, measured earlier, are utilized in order to quantify void sizes. An equivalent diameter, D_{eq}, is defined to classify the void size for each void as:

$$D_{eq} = \sqrt{\frac{4A}{\pi}}, \tag{5}$$

where A is the measured area of the void. Size distributions of inner and surface voids based on D_{eq} are shown in figure 5. Both distributions are one-tailed distributions, contrasting with typical bimodal void distributions observed in fiber reinforced molded composites [14], where the first peak represents inter-tow micro-voids and the second intra-tow macro-voids. As mentioned earlier, the range of modified capillary numbers that are calculated as 0.13 to 1.15 implies that the formed voids are primarily inter-tow micro-voids [8], which explains the presence of fewer large macro-voids. However, size distributions of inner and surface voids are considerably different. The size distribution of inner voids presents a larger peak, with a higher maximum frequency of 21.96% for voids with equivalent diameter between 30 and 40 μm, and a narrower tail, with no voids having an equivalent diameter larger than 140 μm. The size distribution of surface voids depicts a maximum frequency of 18.56% for voids with equivalent diameter between 50 and 60 μm, and existence of voids even larger than 200 μm. These size distributions show clearly that surface layer voids are generally larger than inner voids. Surface layer also contains some very large voids (over 200 μm) in contrast with inner layer that does not contain any void with an equivalent diameter larger than 137.62 μm. This difference in size distribution of the two layers is compensated by an opposite difference in void density. Inner voids shows a void density of 10.75 voids per mm^2, while surface voids shows a void density of 9.76 voids per mm^2, thus yielding comparable average void contents of 2.28 and 2.05% for inner and surface layers, respectively. These results are expected as uneven spaces between the preform and the mold walls, and the variation of fluid front velocity between mid-plane and other planes, coupled with poor wettability of the aluminum mold wall pretreated with Teflon mold releasing agent lead to variation in voidage through-the-thickness of the composite disk.

In order to categorize the observed differences in void sizes, three different sizes are defined. Large voids are defined as those voids with an equivalent diameter greater than100 μm, i.e. $D_{eq} > 100$ μm; while voids with an equivalent diameter lower than 50 μm are regarded as small voids. Intermediate equivalent diameter values, i.e. 50 μm $< D_{eq} \leq$ 100 μm, correspond to medium size voids. Figure 6 depicts representative small, medium, and large voids as defined above. Figure 6(a) shows an example of a large void with an equivalent diameter of 141.98 μm. In contrast, figure 6(b) depicts two small voids and one barely medium void. The equivalent diameter of the void at the bottom half of figure 6(b) is measured as 57.05 μm, while the other two voids are measured as 40.69 and 34.73 μm, respectively. Figure 6(c) depicts a medium and a small void. The medium void, D_{eq} = 81.15 μm, is caught between two fiber tows. It should be noted that the void in figure 6(c) is also considered a transition void since it is only adjacent to fiber bundles. With an equivalent diameter of only D_{eq} = 81.15 μm, The small void trapped inside the fiber tow located in the bottom of figure 6(c) is considered a preform void. The image shown in figure 6(d) comprises voids with different sizes (equivalent diameters of 31.29, 122.99, 122.87, 68.37, and 38.04 μm – from top to bottom).

Furthermore, using these three different void sizes, voids from different zones within the composite show a substantial difference in size distribution. This variation in size distribution is shown in figure 7. Relative percentage of large voids is almost the same for all the composite zones. However, presence of medium voids in preform zone show a substantial difference compared to matrix and transition zones. Medium voids form only 28.65% of all voids in preform zone, while they form 61.29 and 67.13% of all voids in matrix and transition zones, respectively. At the same time, an opposite difference in relative percentage of small voids is registered. Small voids make up 65.99% of all voids observed in the preform, while they form only 33.33 and 24.30% of all voids in matrix and transition zones, respectively. This finding concur with previous studies showing that intra-tow voids are usually larger than the inter-tow voids [6,13,14]. However, due to the higher range of modified capillary number in the present study, the sizes of observed intra-voids are closer to those observed for inter-tow voids.

Variation of void shape

Since voids with different shapes are known to induce different failure mechanisms [3], shape distribution within a load-bearing composite becomes important in predicting a part's performance. As figures 2 and 6 depict, different void shapes are encountered in the composite sample. Voids shown in figures 2(b), 2(d), 6(a), and 6(b) are mostly circular. In contrast, the void captured in figure 6(c), and the void caught between fiber bundles in figure 6(d) are more elliptical. The

small void entrapped within the preform in the latter figure and those depicted in figure 2(c) present a different asymmetrical geometry. In order to quantify these differences and categorize void shapes, both geometrical and quantitative void characteristics are combined. First, based on the observed shape, voids are divided into two groups: irregular and regular shapes. Irregular void shapes are defined as those presenting a non-convex planar surface area, that is, one can find two different points within the void that can be connected in a straight line that goes outside the void. The remaining voids are defined as regular. A quantitative measure of geometrical circularity of regular voids is introduced to distinguish between circular and elliptical voids. The data obtained from captured voids is further processed by introducing the shape ratio, R_s, defined for each void as the equivalent diameter obtained from equation (5) divided by the maximum measured length L_{max}, within a void:

$$R_s = \frac{D_{eq}}{L_{\max}} . \tag{6}$$

Since an ideal circle is represented by $R_s = 1$, only voids with shape ratios above 0.95 ($0.95 < R_s \leq 1$) are considered as circular voids (the void shown in figure 6(a) for instance). Voids with shape ratios lower than 0.95 comprise a minor axis smaller than the maximum length. The circular symmetry is lost, and they are better classified as elliptical voids. For example, the void caught between preform bundles in figure 6(d) has a shape ratio of 0.78. Relative percentages of voids with different shapes are depicted in figure 8. Considering the overall composite disk, circular and irregular voids have relative percentages of 37.65 and 34.75%, respectively. Elliptical voids, on the other hand, have the lowest relative occurrence at 27.60%. The inner and surface shape distributions are also investigated in order to determine any potential difference in shape distribution caused by the surface non-uniformity. Figure 8 includes shape distributions of voids encountered within the inner and surface layers. Both layers show a very similar shape distribution of voids. Relative percentages of elliptical voids in inner and surface layers are 26.61 and 28.54%, whereas frequency of circular voids in inner and surface layers is 38.44 and 36.50%, respectively. These results suggest that proximity to the mold surface seem to have no effect on void shape distribution.

Finally, using the shape criteria for voids presented earlier, relative contributions of voids with different sizes to circular, elliptical, and irregular shaped voids are calculated. The resulting relative percentage of voids having different sizes based on shape is presented in figure 9. A distinct difference in size distribution between the three defined void geometries is observed. As large voids occurrence is more or less the same for all the shapes (around 7%), relative percentage of small void jumps from a low 25.31% for circular voids to a high 57.47 % for irregular voids. Medium voids see an opposite trend as their relative percentage goes from a high 67.78% for circular voids to 50.38% for elliptical voids, and to even a low 36.00% for irregular voids. Size distribution of elliptical voids is found similar to the overall size distribution shown in figure 7. Circular and irregular voids, on the other hand, display different size distributions as they are in average larger and smaller, respectively, than the overall void size average. Figure 9 also reveals that irregular voids are mostly small, while circular voids are mostly medium voids. These results can be better understood if zone locations of voids with different shapes are considered. Irregular voids are mostly encountered in the preform zone. Therefore, they are expected to be smaller than the circular voids, which occur mostly in matrix or preform zones.

CONCLUDING REMARKS

Voidage distribution is important for resin transfer molded composites since it dictates overall performance of the product. Microscopic image analysis is utilized to investigate through-the-thickness void distribution for a resin transfer molded, disk-shaped, E-glass/epoxy composite. The results indicate significant void variation through the composite's thickness. Void content, for instance, was found to fluctuate through-the-thickness of the part with a variation as much as 17% of the overall 2.15% void content. Primarily, micro-scale voids are encountered since the mold filling is conducted at relatively high modified capillary numbers. Furthermore, voids are found to be mostly concentrated within or right next to the preform with more than 93% of voids occurring in preform and transition zones. Voids occurring next to the mold surface are found to be larger in average than inner voids, whereas voids within the preform are observed to be smaller in average than voids from other composite zones. Finally, mold walls are found to have no apparent effect on shape distribution of voids through-the-thickness of the composite.

REFERENCES

1. Abraham, D., Matthews, S., and Mcllhagger, R., 1998, "A Comparison of Physical Properties of Glass Fiber Epoxy Composites Produced by Wet Lay-up with Autoclave Consolidation and Resin Transfer Moulding," Composites Part A, 29, pp. 795-801.
2. Judd, N. C. W., and Wright, W. W., 1978, "Voids and Their Effects on the Mechanical Properties of Composites ─ an Appraisal," SAMPE Journal, 14(1), pp. 10-14.
3. Goodwin, A. A., Howe, C. A., and Paton, R. J., 1997, "The Role of Voids in Reducing the Interlaminar Shear Strength in RTM Laminates," Proceedings of ICCM-11, Volume IV, M. L. Scott, Ed, Australian Composite Structures Society, pp. 11-19

4. Harper, B. D., Staab, G. H., and Chen, R. S., 1987, "A Note on the Effect of Voids Upon the Hygral and Mechanical Properties of AS4/3502 Graphite/Epoxy," Journal of Composite Materials, 21, pp. 280-289.
5. Patel, N., and Lee, L. J., 1995, "Effect of Fiber Mat Architecture on Void Formation and Removal in Liquid Composite Molding," Polymer Composites, 16(5), pp. 386-399.
6. Mahale A. D., Prud'Homme, R. K., and Rebenfeld, L., 1992, "Quantitative Measurement of Voids Formed During Liquid Impregnation of Nonwoven Multifilament Glass Networks Using an Optical Visualization Technique," Polymer Engineering and Science, 32(5), pp. 319-326.
7. Patel, N., Rohatgi, V., and Lee, J. L., 1995, "Micro Scale Flow Behavior and Void Formation Mechanism During Impregnation Through a Unidirectional Stitched Fiberglass Mat," Polymer Engineering and Science, 35(10), pp. 837-851.
8. Rohatgi, V., Patel, N., and Lee, J. L., 1996, "Experimental Investigation of Flow Induced Micro-Voids During Impregnation of Unidirectional Stitched Fiberglass Mat," Polymer Composites, 17(2), pp. 161-170.
9. Stabler, W. R., Tatterson, G. B., Sadler, R. L., and El-Shiekh, A. H. M., 1992, "Void Minimization in the Manufacture of Carbon Fiber Composites by Resin Transfer Molding," SAMPE Quarterly, January, pp. 38-42.
10. Chan, A. W., and Morgan, R. J., 1992, "Modeling Preform Impregnation and Void Formation in Resin Transfer Molding of Unidirectional Composites," SAMPE Quarterly, April, pp. 48-52.
11. Chui, W. K., Glimm, J., Tangerman, F. M., Jardine, A. P., Madsen, J. S., Donnellan, T. M., and Leek, R., 1995, "Porosity Migration in RTM." Proceedings of the 9th International Conference of Numerical Methods in Thermal Problems, pp. 1323-1334.
12. Lundström, T. S., 1997, "Measurement of Void Collapse During Resin Transfer Moulding," Composites Part A, 28A, pp. 201-214.
13. Patel, N., and Lee, J. L., 1996, "Modeling of Void Formation and Removal in Liquid Composite Molding. Part I: Wettability Analysis," Polymer Composites, 17(1), pp. 96-103.
14. Patel, N. and Lee, J. L., 1996, "Modeling of Void Formation and Removal in Liquid Composite Molding. Part II: Model Development and Implementation," Polymer Composites, 17(1), pp. 104-114.
15. Binetruy, C., Hilaire, B., and Pabiot, J., 1998 "Tow Impregnation Model and Void Formation Mechanisms During RTM," Journal of composite Materials, 32(3), pp. 223-245.
16. Lundström, T. S., 1996, "Bubble Transport Through Constricted Capillary Tubes with Application to Resin Transfer Molding," Polymer Composites, 17(6), pp. 770-779.
17. Shih, C.-H., and Lee, L. J., 2002, "Analysis of Void Removal in Liquid Composite Molding Using Microflow Models," Polymer Composites, 23(1), pp. 120-131.
18. Lundström, T. S., and Gebart, B. R., 1994, "Influence from Process Parameters on Void Formation in Resin Transfer Molding," Polymer Composites, 15(1), pp.25-33.
19. Choi, J. H. and Dahran, C. K. H., 2002, "Mold Fill Time and Void Reduction in Resin Transfer Molding Achieved by Articulated Tooling," Journal of Composite Materials, 36(19), pp. 2267-2285.
20. Olivero, K. A., Barraza, H. J., O'Rear, E. A. and Altan, M. C., 2002, "Effect of Injection Rate and Post Fill Cure Pressure on Properties of Resin Transfer Molded Disks" Journal of Composite Materials, 36(16), pp. 2011-2028.
21. Barraza, H. J., Hamidi, Y. K., Aktas, L., O'Rear, E. A., and Altan, M. C., 2002, "Porosity Reduction in the High-Speed Processing of Glass Fiber Composites by Resin Transfer Molding (RTM)," Journal of Composite Materials, in press.
22. Ghiorse, S. R., 1991, "A Comparison of Void Measurement Methods for Carbon/Epoxy Composites," U. S. Army Materials Technology Laboratory, Report MTL TR 91-13.

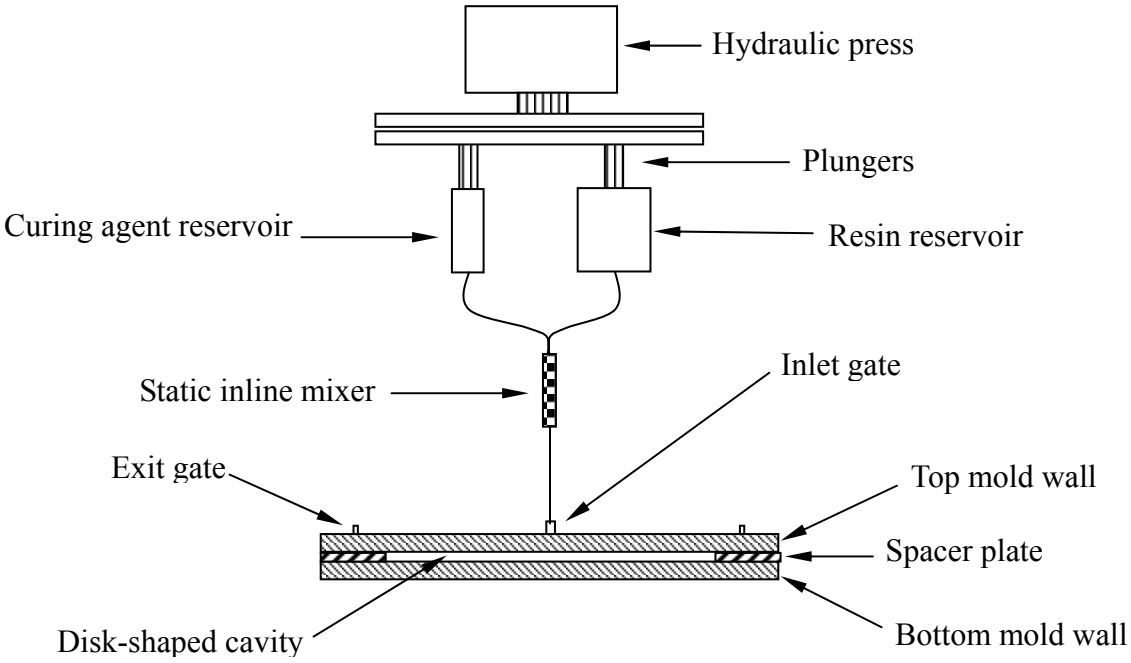

Figure 1: Experimental molding apparatus used to fabricate composite disks.

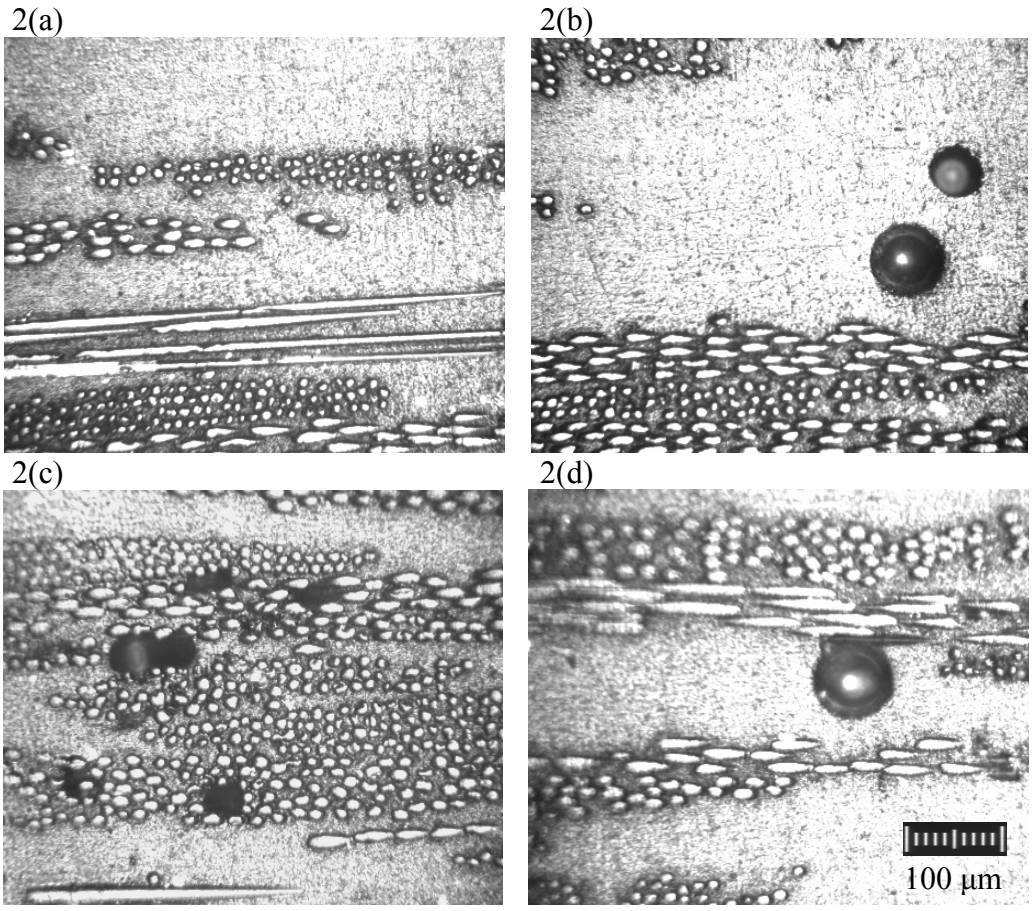

Figure 2: Representative microscopic images obtained at 200 x magnifications depicting examples of voids from different zones: (a) typical composite cross-section with different fiber orientations; (b) two matrix voids; (c) five preform voids; (d) one transition void.

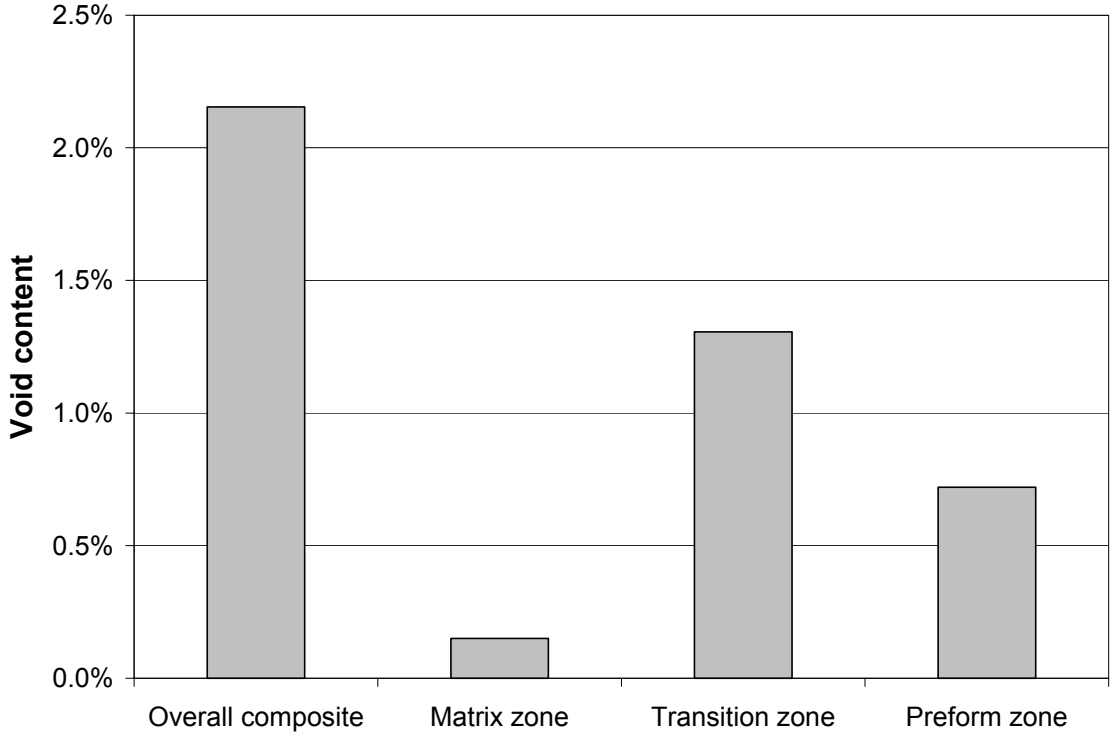

Figure 3: Void content contributions of different locations (void zones) within the composite disk.

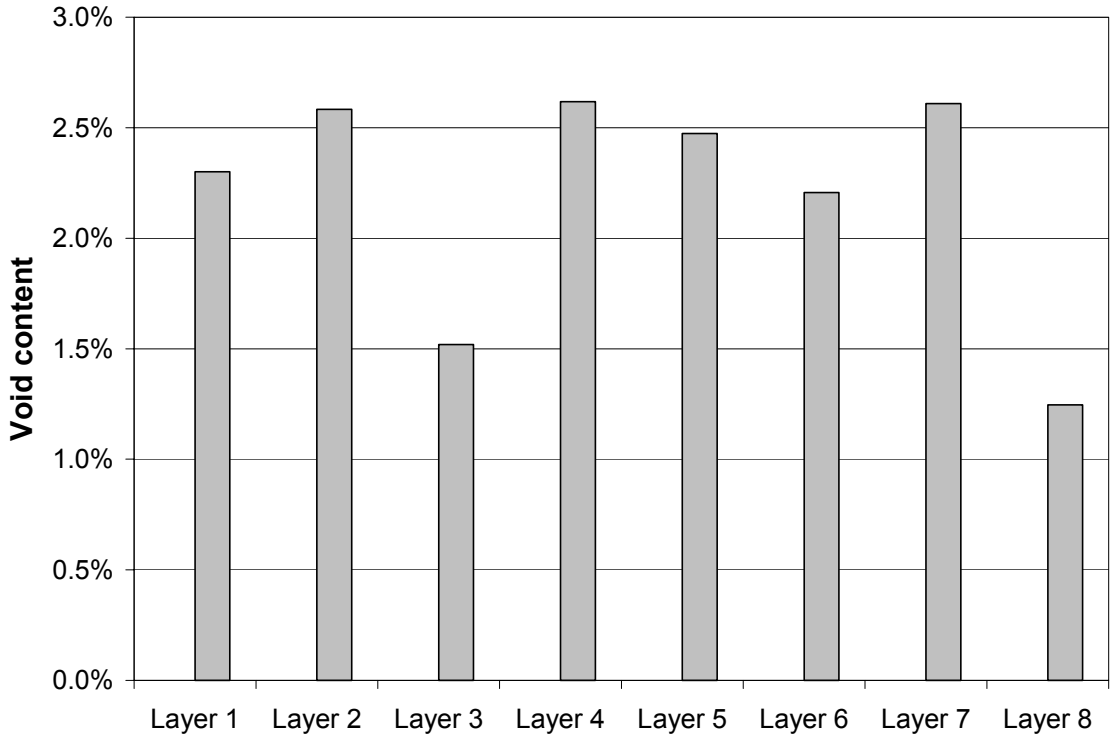

Figure 4: Variation in void content through-the-thickness of the composite disk.

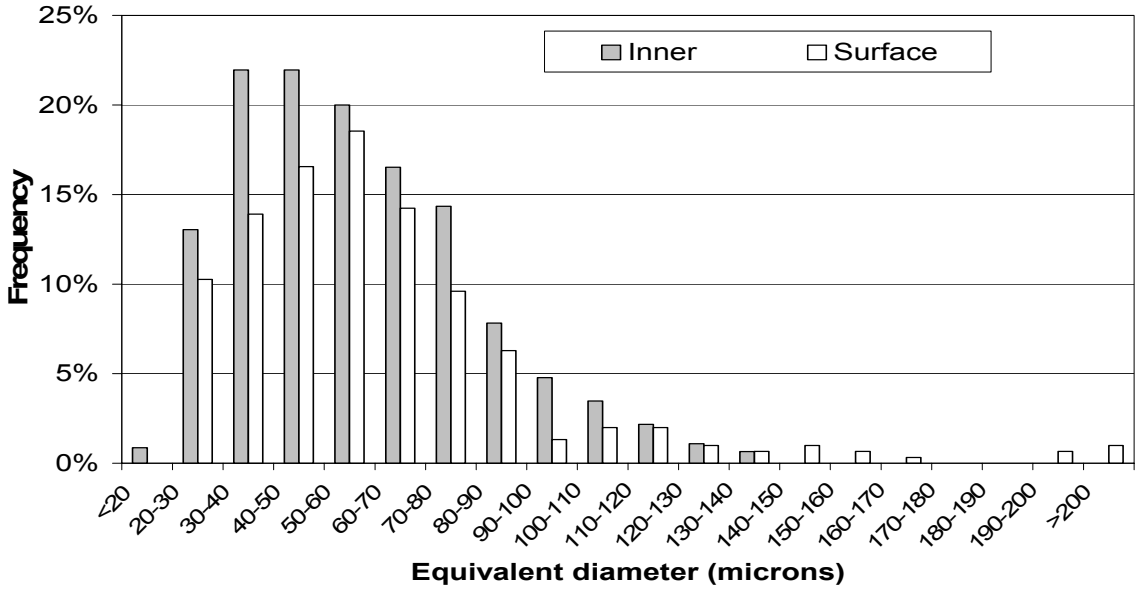

Figure 5: Void size distributions based on equivalent diameter at the surface (next to mold walls) and inner layers.

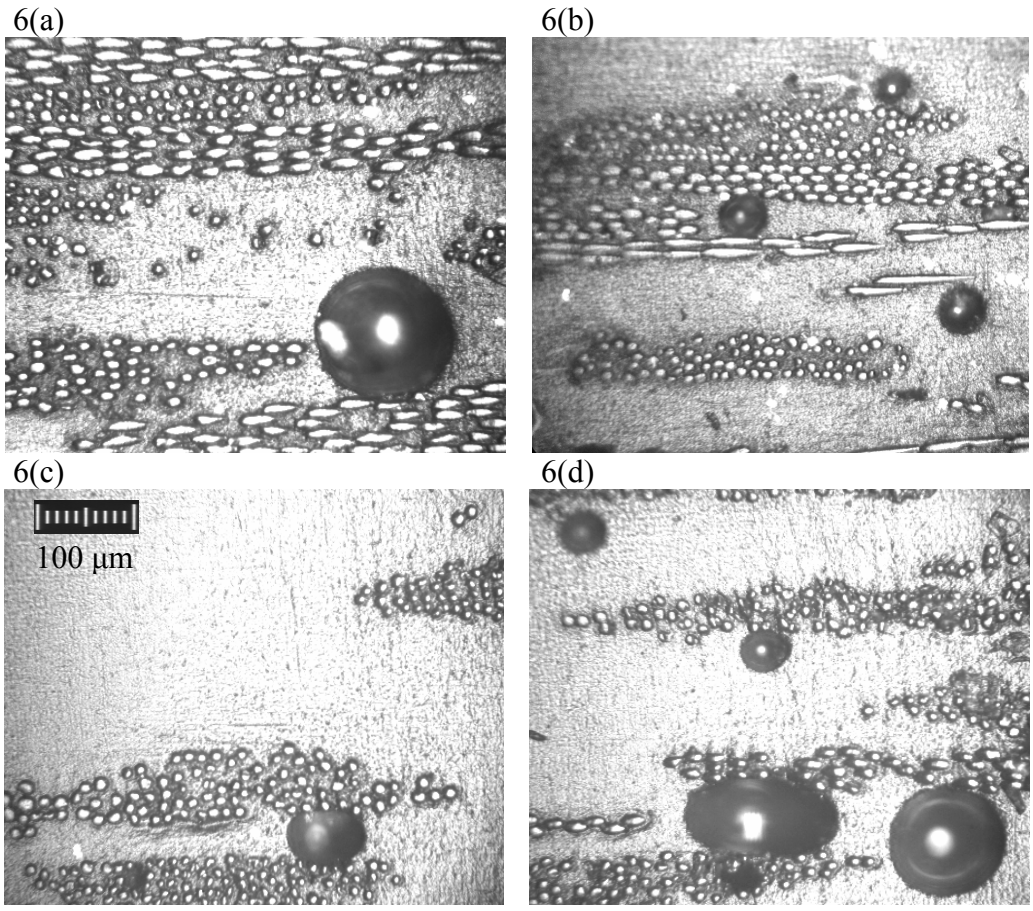

Figure 6: Representative microscopic images obtained at 200 x magnifications depicting voids with different sizes: (a) example of a large void adjacent to a fiber bundle; (b) two small and a barely medium void (from top to bottom); (c) a medium void; (d) voids from different size categories.

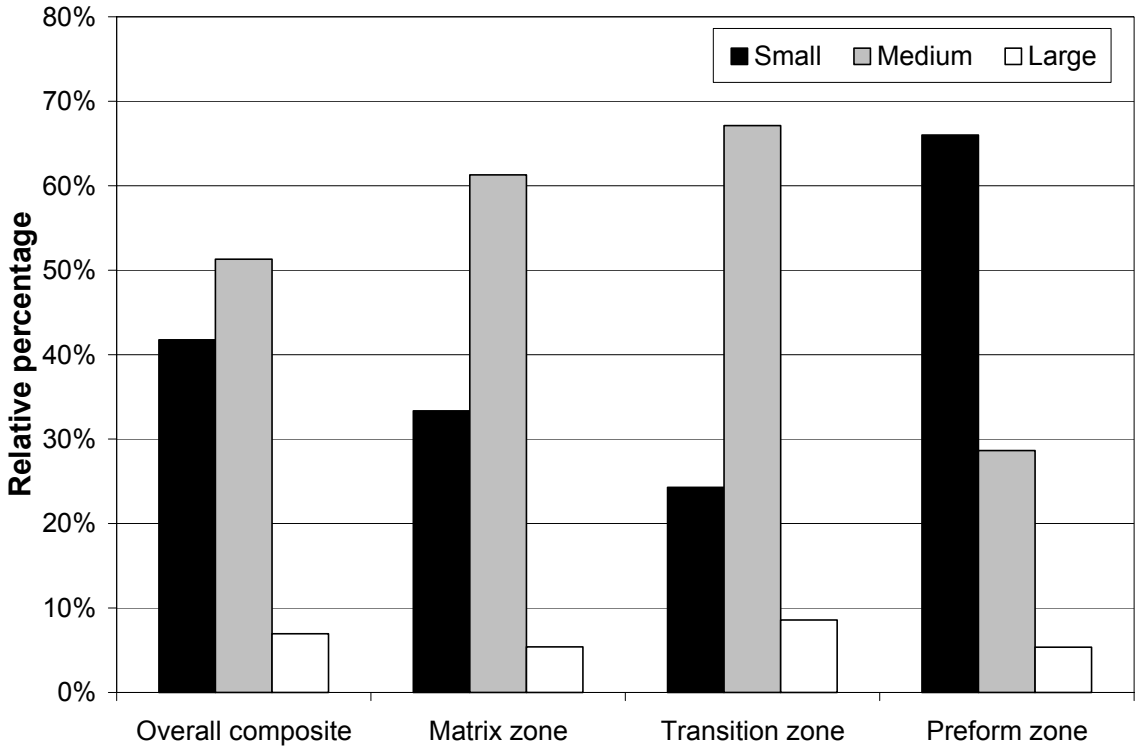

Figure 7: Size distributions of voids from different locations (void zones) within the composite disk.

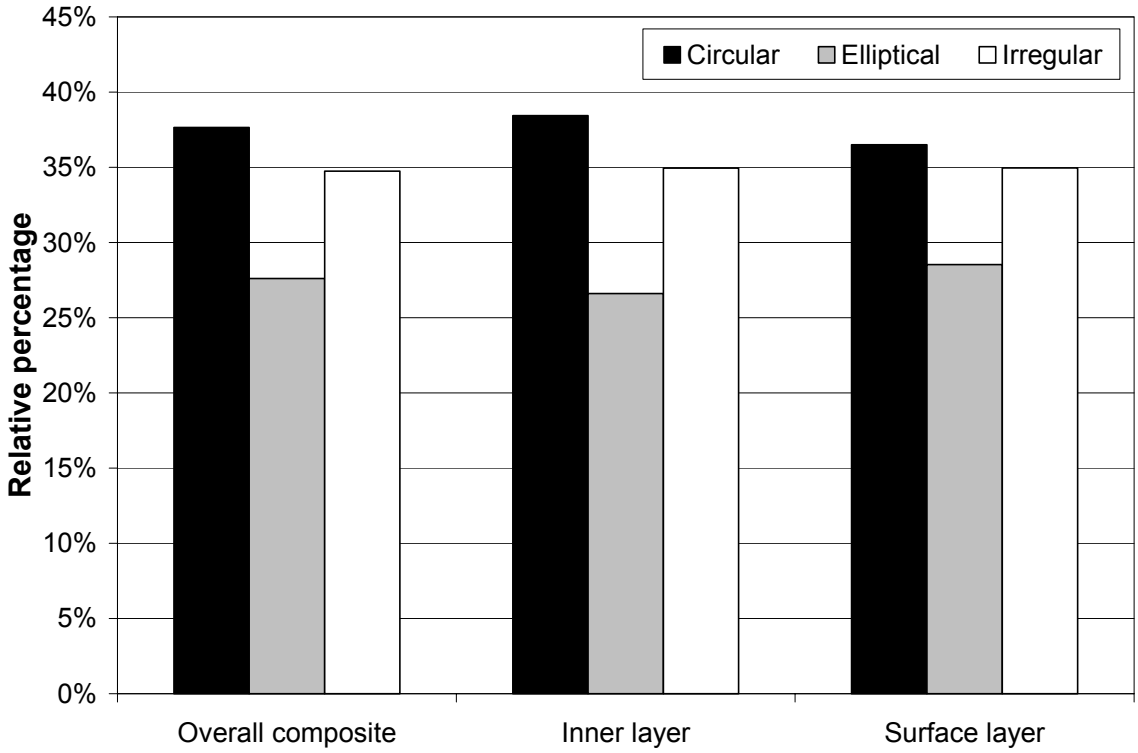

Figure 8: Void content contributions of voids with different shapes.

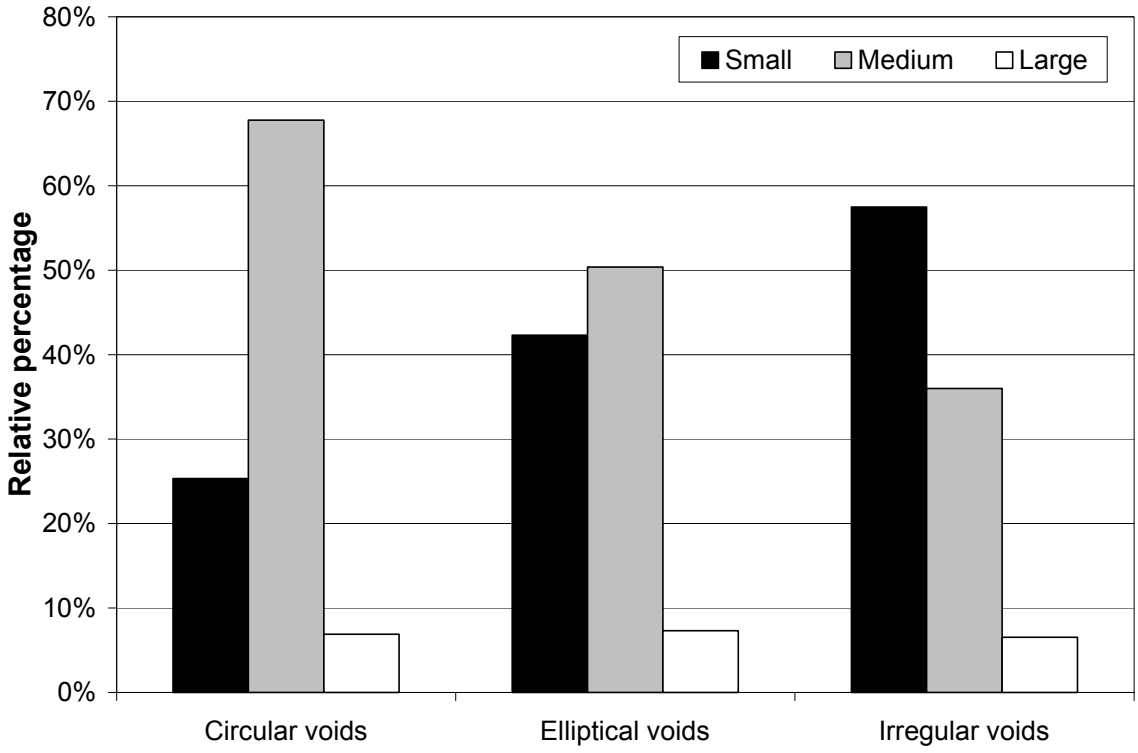

Figure 9: Size distribution of voids with different shapes.